ORIGINAL ARTICLE

Comparison of absorbed doses to the tumoral and non-tumoral liver in HCC patients undergoing ^{99m}Tc-MAA and ^{90}Y-microspheres radioembolization

Nut Noipinit[1,2,5] · Chanan Sukprakun[3] · Punnarai Siricharoen[4] · Kitiwat Khamwan[1,3,5]

Abstract

Purpose This study aimed to determine the absorbed doses in the tumoral-liver and non-tumoral liver of hepatocellular carcinoma (HCC) patients undergoing radioembolization with Yttrium-90 (^{90}Y) resin microspheres, and compared with those derived from ^{99m}Tc-MAA using the partition model.

Methods A total of 42 HCC patients (28 males and 14 females, mean age 65 ± 11.51 years) who received 45 treatment sessions with ^{90}Y-microspheres between 2016 and 2021 were included. Pre-treatment ^{99m}Tc-MAA and post-treatment ^{90}Y-bremsstrahlung SPECT/CT were acquired for each patient. Semi-automated segmentation of regions of interest (ROIs) was performed using MIM Encore software to determine the tumor-liver ratio (TLR) encompassing the liver volume, tumoral-liver, and lungs, and verified by both nuclear medicine physician and interventional radiologist. A partition dosimetry model was used to estimate the administered activity of ^{90}Y-microspheres and the absorbed doses to the tumoral-liver and non-tumoral liver. The student's paired t test and Bland–Altman plot were used for the statistical analysis.

Results The mean TLR values obtained from ^{99m}Tc-MAA SPECT/CT and ^{90}Y-bremsstrahlung SPECT/CT were 4.78 ± 3.51 and 2.73 ± 1.18, respectively. The mean planning administered activity of ^{90}Y-microspheres based on ^{99m}Tc-MAA SPECT/CT was 1.56 ± 0.80 GBq, while the implanted administered activity was 2.53 ± 1.23 GBq (p value < 0.001). The mean absorbed doses in the tumoral-liver estimated from ^{99m}Tc-MAA and ^{90}Y-bremsstrahlung SPECT/CT were 127.44 ± 4.36 Gy and 135.98 ± 6.30 Gy, respectively. The corresponding mean absorbed doses in the non-tumoral liver were 34.61 ± 13.93 Gy and 55.04 ± 16.36 Gy.

Conclusion This study provides evidence that the administered activity of ^{90}Y-microspheres, as estimated from ^{90}Y-bremsstrahlung SPECT/CT, was significantly higher than that estimated from ^{99m}Tc-MAA SPECT/CT resulted in increased absorbed doses in both the tumoral-liver and non-tumoral liver. However, ^{99m}Tc-MAA SPECT/CT remains a valuable planning tool for predicting the distribution of ^{90}Y-microspheres in liver cancer treatment.

Keywords ^{90}Y-microspheres · ^{99m}Tc-MAA SPECT/CT · ^{90}Y-bremsstrahlung SPECT/CT · Partition model · SIRT · Absorbed doses

✉ Kitiwat Khamwan
kitiwat.k@chula.ac.th

1 Medical Physics Program, Faculty of Medicine, Chulalongkorn University, Bangkok, Thailand

2 Division of Nuclear Medicine, Department of Radiology, King Chulalongkorn Memorial Hospital, The Thai Red Cross Society, Bangkok, Thailand

3 Division of Nuclear Medicine, Department of Radiology, Faculty of Medicine, Chulalongkorn University, Bangkok, Thailand

4 Department of Computer Engineering, Faculty of Engineering, Chulalongkorn University, Bangkok, Thailand

5 Chulalongkorn University Biomedical Imaging Group, Department of Radiology, Faculty of Medicine, Chulalongkorn University, Bangkok, Thailand

Introduction

According to the report on global cancer incidence from International Agency of world health organization for cancer research in 2020, liver cancer ranks as the sixth most common cancer worldwide and is the third leading cause of death, surpassed only by colorectal cancer and lung cancer [1]. Notably, gastrointestinal cancers, including esophageal, gastric, and liver cancers, were found to be more prevalent in Asia compared to other regions [2]. In Thailand, liver cancer holds the unfortunate position of being the primary cause of death. A selective internal radiation therapy (SIRT) using Yttrium-90 (^{90}Y) microsphere is a frequently employed technique in interventional radiology for the treatment of hepatocellular carcinoma (HCC), particularly for cases where surgical resection is not possible [3]. ^{90}Y is a pure beta-emitting radionuclide with a half-life of 64.2 h. Approximately 99.9% of its emissions consist of beta particles with an average energy of 0.937 MeV that disintegrates into stable zirconium-90 (^{90}Zr), and have a maximum soft tissue range of approximately 1.1 cm [4, 5]. This unique combination of properties makes ^{90}Y well-suited for use in radioembolization and other targeted radionuclide therapies, as it allows for focused radiation delivery to the tumor regions while minimizing damage to surrounding healthy tissues.

Prior to SIRT treatment, patients undergo a ^{99m}Tc-macroaggregated albumin (MAA) scan, which includes whole-body planar imaging and SPECT/CT. The imaging data obtained from the ^{99m}Tc-MAA scan are used to calculate the lung shut fraction (LSF), tumor-to-liver ratio (TLR), and estimate the appropriate activity of ^{90}Y-microspheres. Subsequently, patients undergo a ^{90}Y-bremsstrahlung SPECT/CT scan after treatment to verify accurate selection of tumoral locations. Therefore, it is crucial to evaluate not only the treatment efficacy of SIRT using ^{90}Y-microspheres but also its safety and potential side effects [5–7].

To determine ^{90}Y administered activity (AA) and dosimetry, commonly used calculation models include the medical internal radiation dose (MIRD) [8–11], body surface area (BSA), and the partition model method. Among these methods, the partition model is the most widely employed, as it allows for the separation of the liver into distinct compartments, including the tumoral-liver and non-tumoral liver regions. By incorporating the AA of ^{90}Y-microspheres and the TLR, which represents the relative uptake in these regions, the dosimetry formula provides estimates of the absorbed doses delivered to each compartment during the SIRT procedure. This approach ensures that the radiation dose distribution is more patient specific and takes into account the differential uptake in tumoral and non-tumoral liver tissues [4–7, 12]. Given the increasing interest in personalized radionuclide therapy, the establishment of a strong and reliable relationship between the prescribed and the pre-treatment doses is essential [13–15].

In this study, we aim to determine the administered activity and absorbed doses in the tumoral-liver and non-tumoral liver of HCC patients who underwent post-treatment ^{90}Y-microspheres SIRT, utilizing ^{90}Y-bremsstrahlung SPECT/CT imaging based on the partition model. The results were then compared with the ^{99m}Tc-MAA pre-treatment to validate the accuracy of the prescribed treatment planning dosimetry for both tumoral and non-tumoral liver regions.

Materials and methods

Patients

This study was approved from our institutional review board (IRB) to collect retrospective data from HCC patients who underwent ^{99m}Tc-MAA and ^{90}Y-bremsstrahlung SPECT/CT scans for SIRT with ^{90}Y-microspheres at King Chulalongkorn Memorial Hospital (KCMH) between 2016 and 2021. The study's inclusion criteria consisted of HCC patients with radiologically proven liver cancer who did not undergo surgical treatment, and for whom both pre-treatment ^{99m}Tc-MAA SPECT/CT images and post-treatment ^{90}Y-bremsstrahlung SPECT/CT images were available. Patients with a lung shunt $\geq 20\%$ and those with diffuse infiltrative liver metastases were excluded from this study.

Radioembolization and image acquisition

All patients were injected ^{99m}Tc-MAA for pre-treatment planning at the Interventional Radiology Unit. Hepatic angiography was performed after selectively occluding single or multiple accessory hepatic arteries using embolized coils. A slow administration of 185 MBq of ^{99m}Tc-MAA in 5–6 mL of physiologic solution was injected via the catheter, and its precise position was recorded on the angiogram to facilitate catheter repositioning during the treatment session. SPECT/CT images were then acquired at the Nuclear Medicine Division using the Symbia Truepoint T6 (Siemens Healthineers, Germany) or Discovery NM/CT 670 (GE Healthcare, USA) SPECT/CT system within 60 min to evaluate the lung shunt fraction and estimate ^{90}Y-microspheres injected activity and dosimetry. For image acquisition, a low energy high-resolution collimator and an energy window at 140 keV $\pm 7.5\%$ were used. The SPECT images were acquired with a matrix size of 128×128 and 32 projections (30 s/projection). Flash 3D ordered-subset expectation maximization

(OSEM), with 4 iterations and 8 subsets, and scatter correction were applied for image reconstruction. Low-dose CT was acquired for attenuation correction. The tumor volume, non-tumor volume, and TLR were subsequently determined, utilizing information obtained from contrast-enhancement CT images.

To obtain post-SIRT imaging, ^{90}Y-bremsstrahlung SPECT/CT imaging was performed on the same scanner system as the ^{99m}Tc-MAA SPECT/CT. For the ^{90}Y-bremsstrahlung SPECT/CT acquisition, a medium energy collimator was employed, and the energy window was set at 78 keV $\pm$ 15%. The image acquisition parameters consisted of a 128×128 matrix with 32 projections (30 s/projection), and reconstructed using Flash 3D OSEM, with 5 iterations and 8 subsets. Attenuation and scatter correction were also applied.

Tumoral and non-tumoral liver segmentation

The co-registration of ^{99m}Tc-MAA SPECT and ^{90}Y-bremsstrahlung SPECT with CT images, as well as the delineation of tumoral-liver, non-tumoral liver, and lung compartments, were performed using MIM Encore software version 7.1.3 (MIM Software Inc., Cleveland, Ohio), as illustrated in Fig. 1. In this study, lesions and lobar contouring were performed using a semi-automated segmentation method. Initially, a 50% thresholding of the maximum intensity on the SPECT/CT images was used to delineate the tumoral-liver regions. If the contours did not cover the tumor region adequately, the threshold value for each VOI was adjusted following the boundaries of the tumors individually. Additionally, the MIM software could automatically generate contours by referencing each patient's prior information from preceding slices, facilitating the contouring of VOI. Although the segmentation mainly performed on SPECT/CT, the contrast-enhanced CT images acquired from diagnostic radiology were additionally used as a reference for the tumoral-liver VOI. This reference aided in verifying the accuracy of tumor lobe distribution and size segmentation, with the objective of ensuring precise delineation of tumoral regions. The non-tumoral liver volume was derived by subtracting the tumoral-liver volume from the treated liver lobe volume. All segmented volumes of tumoral and non-tumoral liver were finalized through a consensus between a certified nuclear medicine physician and an interventional radiologist. In the case of the lung compartments, regions were semi-automatically defined using a threshold level of Hounsfield unit (HU).

Administered activity and dosimetry calculation

The tumor-to-liver ratio (TLR) for each patient was calculated by analyzing the radioactivity uptake in the
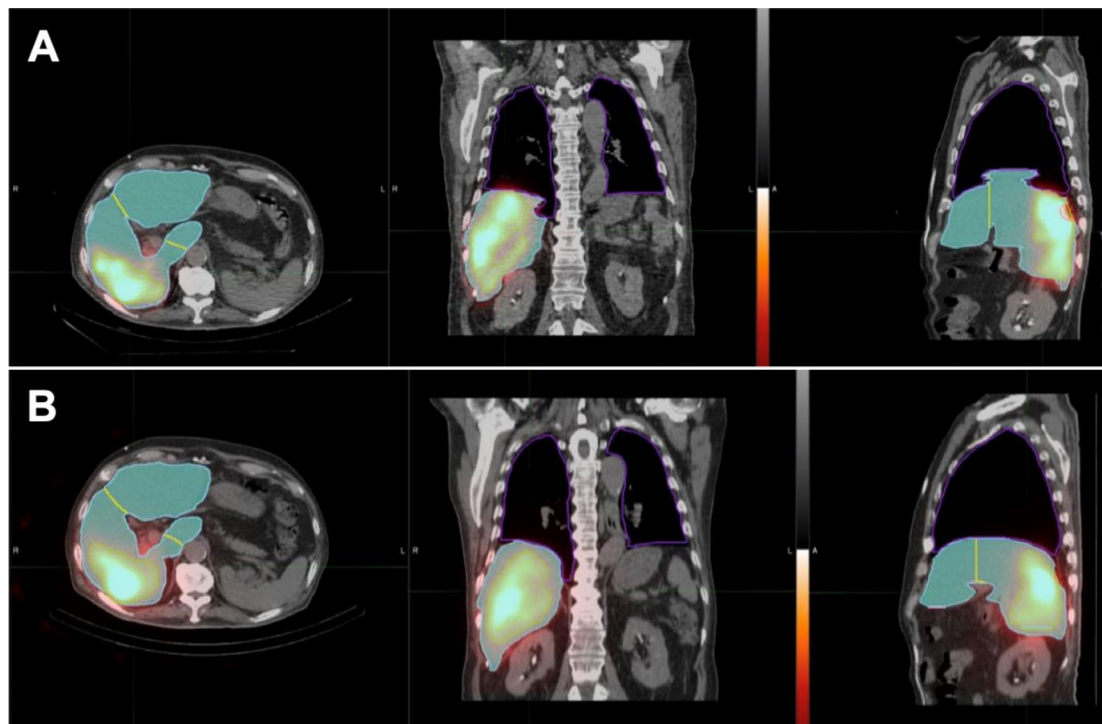

Fig. 1 Example of semi-automated delineation of liver, tumoral-liver and lung regions using MIM Encore software in same patient on co-registration images in transaxial, coronal and sagittal planes. **A** ^{99m}Tc- MAA SPECT/CT images and **B** ^{90}Y- bremsstrahlung SPECT/CT images. The yellow lines indicate the partition that separates each lobe

tumoral-liver and non-tumoral liver regions, measured per unit mass of each respective region. The TLR can be calculated using Eq. (1) as follows [16]:

$$TLR = \frac{A_T(GBq)/m_T(kg)}{A_N(GBq)/m_N(kg)} \tag{1}$$

where A_T is the uptake activity within the tumoral-liver compartment, m_T is the mass of the tumoral-liver compartment, A_N is the uptake activity within the non-tumoral liver compartment, and m_N is the mass of the non-tumoral liver compartment. A density factor of 1.03 g/mL was applied to convert the volume of the tumoral-liver and non-tumoral liver into mass [17].

Lung shunting fraction (LSF) was calculated using whole-lung SPECT/CT scan to assess the presence of extrahepatic blood vessels that may direct a vascular path to the lungs, resulting in lung irradiation by ^{90}Y microspheres. LSF is defined as the ratio of total counts in lungs divided by the total counts in both the liver and lungs, and it is calculated using the following equation:

$$LSF = \frac{C_{lungs}}{C_{liver} + C_{lungs}} \tag{2}$$

where C_{lungs} represents the total counts in lungs, and C_{liver} represents the total counts in liver. Subsequently, the partition dosimetry model was employed to calculate the administered activity of ^{90}Y using Eq. (3) [18, 19]:

$$A(GBq) = \frac{D_T(Gy) \times [(TLR \times m_T(kg)) + m_N(kg)]}{49.67 \times (1 - LSF)} \tag{3}$$

where A is administered activity of ^{90}Y, D_T denotes the dose to the tumor, defined at a minimum of 120 Gy as the target dose to the treated liver lobe, TLR is the relative uptake of tumoral and non-tumoral liver ratio, m_N represents the mass of the non-tumoral liver compartment, and m_T represents the mass of the tumoral-liver compartment.

The absorbed doses to the tumoral-liver (D_T) and non-tumoral liver (D_{NL}), derived from the administered activity of ^{99m}Tc-MAA, were calculated using Eqs. (4) and (5) as follows [18, 19]:

$$D_{NL}(Gy) = \frac{A(GBq) \times 49.67 \times (1 - LSF)}{[(TLR \times m_T(kg)) + m_N(kg)]} \tag{4}$$

$$D_T(Gy) = TLR\, D_{NL}(Gy) \tag{5}$$

where A is an administered activity, TLR is the tumor-liver ratio, representing the relative uptake of the ^{99m}Tc-MAA in the tumoral and non-tumoral liver regions as mentioned previously, m_N is the mass of the non-tumoral liver compartment, m_T is the mass of the tumoral-liver compartment.

For the absorbed doses for tumoral and non-tumoral liver obtained from ^{90}Y-microspheres radioembolization, the dosimetry was calculated using ^{90}Y-bremsstrahlung SPECT/CT images, which was based on the partition model formula following Eq. (4) and (5) similar to ^{99m}Tc-MAA dosimetry calculation.

Statistical analysis

The student's t test was used to determine the statistical difference of ^{90}Y administered activity and absorbed dose in the tumoral-liver and non-tumoral liver between ^{99m}Tc-MAA and ^{90}Y-microspheres radioembolization. P values < 0.05 were considered statistically significant in this study. To assess the agreement of ^{90}Y administered activity and absorbed doses in the tumoral-liver and non-tumoral liver between ^{99m}Tc-MAA and ^{90}Y post-treatment SPECT/CT, Bland–Altman plots were employed for the analysis.

Results

Patients

A total of 45 treatment sessions conducted on 42 HCC patients (28 males and 14 females, with a mean age of 65 ± 11.51 years) were included in this study. All patients underwent ^{90}Y-microspheres SIRT, and pre-treatment ^{99m}Tc-MAA and post-treatment ^{90}Y-bremsstrahlung SPECT/CT scans were obtained. All treatment sessions were included in the analysis to determine the administered activity and absorbed dose in both the tumoral-liver and non-tumoral liver regions. The clinical characteristics of the patients are summarized in Table 1.

Table 1 Patient's demographics and clinical characteristics

Characteristics	Overall
Patients (n)	42
Age (year)	65 ± 11.51
Range (year)	36–85
Gender	
Male	28 (66.67%)
Female	14 (33.33%)
Treatment sessions	45
Liver lobe treated	
Right	22 (48.89%)
Left	4 (8.89%)
Both	19 (42.22%)
Mean tumor volume (mL)	325.09 ± 229.79
Mean liver volume (mL)	1761.33 ± 584.64

Dosimetry

According to the TLR results calculated by the MIM software, the mean TLR values obtained from ^{99m}Tc-MAA SPECT/CT and ^{90}Y-bremsstrahlung SPECT/CT were 4.78 ± 3.51 (range 1.9–18.7) and 2.73 ± 1.18 (range 1.7–7.2), respectively. For the partition model calculations, the mean ^{90}Y administered activity estimated based on ^{99m}Tc-MAA was 1.56 ± 0.80 GBq (range 0.22–3.53), while the mean ^{90}Y administered activity estimated by ^{90}Y-bremsstrahlung SPECT/CT was 2.53 ± 1.23 GBq (range 0.76–5.66).

The mean absorbed doses to the tumoral-liver estimated from ^{99m}Tc-MAA and ^{90}Y-bremsstrahlung SPECT/CT were 127.44 ± 4.36 Gy (range 121.33–141.68) and 135.98 ± 6.30 Gy (range 126.98–156.45), respectively. The mean absorbed doses to the non-tumoral liver estimated from ^{99m}Tc-MAA and ^{90}Y-bremsstrahlung SPECT/CT were 34.61 ± 13.93 Gy (range 6.49–63.97) and 55.04 ± 16.36 Gy (range 20.58–78.23), respectively. Figure 2 depicts the box plot illustrating the TLR, administered activity, absorbed doses in tumoral and non-tumoral liver obtained from ^{99m}Tc-MAA and ^{90}Y-^{90}Y-bremsstrahlung SPECT/CT. It was found that the TLR, administered activity of ^{90}Y, absorbed dose in tumoral-liver and non-tumoral liver were statistically significant difference (p value < 0.001) between ^{99m}Tc-MAA SPECT/CT and ^{90}Y-bremsstrahlung SPECT/CT as summarized in Table 2.
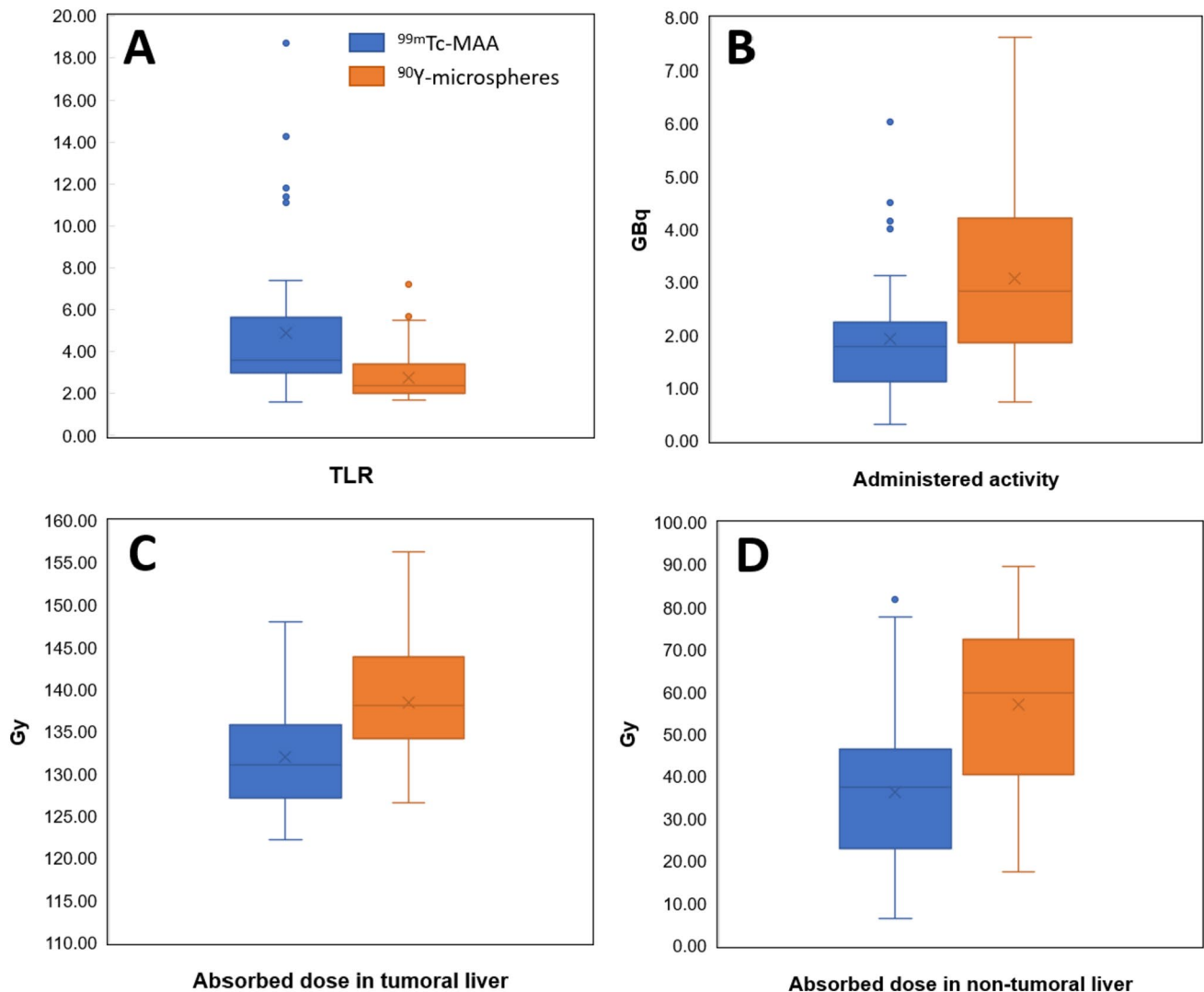

Fig. 2 Box plot represents a comparison of results between ^{99m}Tc-MAA and ^{90}Y-bremsstrahlung SPECT/CT values; **A** TLR, **B** administered activity, **C** absorbed dose in tumoral liver, **D** absorbed dose in non-tumoral liver

Table 2 Summary results between ^{99m}Tc-MAA and ^{90}Y-microspheres radioembolization

Characteristics	^{99m}Tc-MAA	^{90}Y-microspheres	p value
TLR	4.90 ± 3.49 (2.0–18.7)	2.77 ± 1.18 (1.7–7.2)	< 0.001
Administered activity of ^{90}Y-microspheres (GBq)	1.82 ± 0.93 (0.32–4.15)	3.07 ± 1.53 (0.82–6.54)	< 0.001
Absorbed dose in tumoral-liver (Gy)	127.33 ± 4.49 (120.00–141.68)	136.04 ± 6.24 (126.98–156.45)	< 0.001
Absorbed dose in non-tumoral liver (Gy)	34.06 ± 13.72 (6.49–63.97)	55.23 ± 15.94 (20.58–76.48)	< 0.001

Agreement between ^{99m}Tc-MAA and ^{90}Y-bremsstrahlung SPECT/CT

The Bland–Altman plots, which illustrate the agreement and discrepancies in ^{90}Y administered activity, as well as the absorbed dose in the tumoral-liver and non-tumoral liver, estimated from ^{99m}Tc-MAA SPECT/CT pre-treatment planning in comparison to ^{90}Y-bremsstrahlung SPECT/CT post-treatment are given in Fig. 3. The mean difference of -1.13 GBq (95% CI − 2.51 to 0.26) was found in administered activity. For absorbed dose in tumoral-liver, the mean difference was -8.71 Gy (95% CI − 19.52 to 2.10). The highest difference in absorbed dose, − 21.17 Gy (95% CI − 48.24 to 5.90), was observed in the non-tumoral liver.

Discussion

The primary goal of ^{90}Y SIRT treatment for unresectable HCC is to optimize the dose delivered to the tumoral-liver while minimizing the dose to the non-tumoral liver and preserving liver parenchyma. During this process, it is essential to ensure that the tumor receives at least the recommended mean absorbed dose while keeping the normal liver tissue below or equal to the safety threshold of 40 Gy [5, 20]. However, the determination of standardized tumor mean dose thresholds remains a subject of debate. Previous literatures suggest mean target absorbed doses ranging from 91 to 250 Gy for HCC and 40–60 Gy for colorectal cancer metastases [21–23]. For neuroendocrine tumor liver metastases,
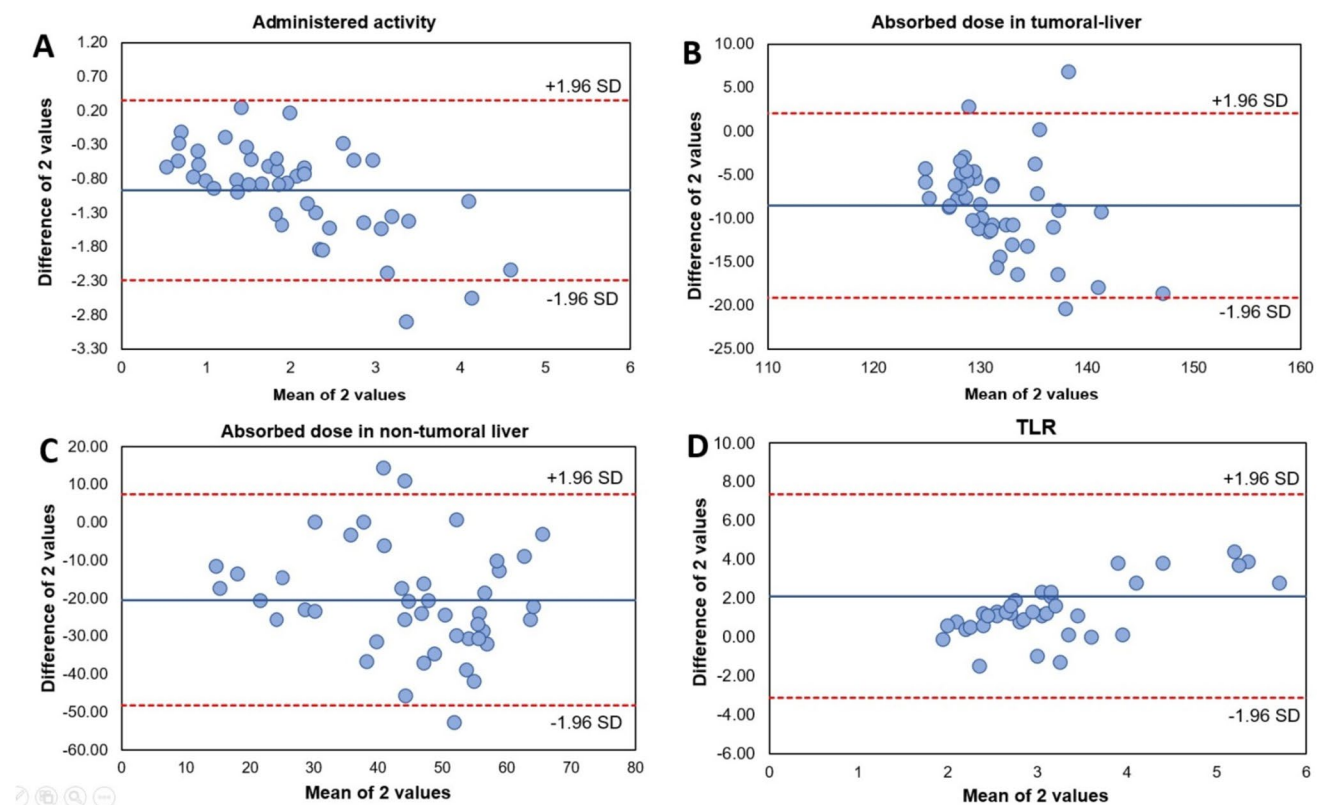

Fig. 3 Bland–Altman plots of agreement and discrepancies between pre-treatment planning ^{99m}Tc-MAA and post-treatment ^{90}Y-microspheres embolization. **A** Administered activity, **B** absorbed dose in tumoral-liver, **C** absorbed dose in non-tumoral liver, and **D** TLR

utilizing ^{99m}Tc-MAA SPECT/CT, an estimated absorbed dose greater than 191.3 Gy has shown promise in predicting treatment response with high sensitivity and specificity [24, 25]. Nonetheless, the accuracy of dosimetry in both tumoral-liver and non-tumoral liver is dependent on the dosimetry method employed and the TLR, which is influenced by the precision and consistency of tumoral and non-tumoral liver contouring. Addressing these aspects is critical in achieving therapeutic success in ^{90}Y SIRT for HCC.

The results from this study demonstrated significant differences in the TLRs obtained from ^{90}Y-bremsstrahlung SPECT/CT compared to those obtained from ^{99m}Tc-MAA SPECT/CT (*p* value < 0.001), consistent with previous literature [7, 16, 26, 27]. The higher TLRs observed from ^{99m}Tc-MAA SPECT/CT could be attributed to the potential challenges in defining the region boundary in ^{90}Y-bremsstrahlung SPECT/CT. The difference may result from the inherent characteristics of each imaging technique, which can influence the accuracy of delineating the tumoral-liver region. Several factors were found to influence the distribution of ^{90}Y-microspheres within the tumor and normal liver tissue, including catheter tip position and prior therapeutic conditions [28]. Additionally, differences in particle size, the embolizing effect of ^{90}Y-microspheres, and the inhomogeneous activity distribution in normal liver tissue could contribute to the observed discrepancies. Despite the lower mean TLR values obtained from ^{90}Y-bremsstrahlung SPECT/CT compared to ^{99m}Tc-MAA SPECT/CT, the variation (standard deviation) of mean TLR obtained from ^{90}Y-bremsstrahlung SPECT/CT was lower than that from ^{99m}Tc-MAA SPECT/CT. These observations might be explained by the mentioned factors affecting the distribution patterns. Nonetheless, the study results indicated a good correlation (r = 0.80) between the TLR values obtained from

^{99m}Tc-MAA and ^{90}Y-bremsstrahlung SPECT/CT as shown in Fig. 3D, suggesting that ^{99m}Tc-MAA SPECT/CT remains a viable pre-treatment planning tool for estimating the distribution of ^{90}Y-microspheres in both tumoral-liver and non-tumoral liver regions.

According to the European Association of Nuclear Medicine (EANM) guideline [5, 7], the prescribed absorbed doses for targeted tumors should be ≥ 100–120 Gy, while the dose for normal liver should be maintained below 40 Gy. In our study, the absorbed doses calculated from ^{99m}Tc-MAA SPECT/CT and ^{90}Y-bremsstrahlung SPECT/CT resulted in a mean absorbed dose of ≥ 100 Gy in the tumoral-liver, meeting the EANM guideline recommendations. However, a substantial difference was observed in the mean absorbed dose in the non-tumoral liver when estimated from ^{90}Y-bremsstrahlung SPECT/CT compared to the planning with ^{99m}Tc-MAA, with the former being approximately 37% higher. This discrepancy might be attributed to certain limitations of ^{90}Y-bremsstrahlung SPECT/CT images, such as image quality issues caused by scatter radiation, photopeak acquisition, and the imaging acquisition process [29–31]. Despite the significant difference in tumor outlines observed between these two image sessions, leading to distinct dosimetry, the issue was addressed through verification by interventional radiologist and nuclear medicine physician to ensure accurate delineation of tumor regions.

Our study found that the mean absorbed doses in both the tumoral liver and non-tumoral liver were comparable to previous studies findings [21, 22, 24, 25, 32]. A summary of the absorbed doses obtained from our study on HCC patients treated with ^{90}Y-microspheres, in comparison with literatures, is provided in Table 3. Regarding the outlier observed in the Bland–Altman plot, the administered activity (Fig. 3A) obtained from ^{99m}Tc-MAA was underestimated

Table 3 Comparison of the findings from previous studies with the results of this study on HCC patients treated with ^{90}Y-microspheres

Study	Subjects	Activity prescription method	Tumor dosimetry assessment	Findings
Kao et al. [21]	Unresectable HCC (*n* = 10)	Partition model	^{99m}Tc-MAA SPECT	Mean Tumor ≥ 91 Gy, Non-tumor ≤ 51 Gy
Levillain et al. [22]	Unresectable Primary and secondary liver cancer (*n* = 58)	Multiple	^{99m}Tc-MAA SPECT	Tumor 100–120 Gy and non-tumor 40 Gy
Chansanti et al. [24]	Unresectable mNET (*n* = 15)	Partition model	^{99m}Tc-MAA SPECT	Predictor of response (191.3 Gy), 83% sensitivity and 93% specificity. < 72.8 Gy predicted no response with 100% sensitivity
Gnesin et al. [25]	Unresectable HCC (*n* = 25)	Partition model	^{90}Y-PET 3D	Mean Tumor 122 Gy and Non-tumor 47 Gy
Levillain et al. [32]	Unresectable and chemorefractory (*n* = 58)	BSA or partition model	^{99m}Tc-MAA SPECT	Mean tumor 86 Gy
This study	Unresectable HCC (*n* = 42)	Partition model	^{99m}Tc-MAA SPECT	Mean Tumor 127 Gy and Non-tumor 34 Gy

compared to ^{90}Y-bremsstrahlung. In contrast, the absorbed doses in the tumoral-liver and non-tumoral liver obtained from ^{99m}Tc-MAA were overestimated compared to ^{90}Y-bremsstrahlung, as illustrated in Fig. 3B and C, respectively. This discrepancy raises concerns about potential side effects and toxicity in the non-tumoral liver if absorbed doses are increased. In some cases, interventional radiologists may opt to increase the ^{90}Y administered activity beyond the planning with ^{99m}Tc-MAA, resulting in higher absorbed doses in the tumoral-liver and non-tumoral liver, as seen in ^{90}Y-bremsstrahlung SPECT/CT. Despite these variations, it is noteworthy that the median survival rate of 11 months after ^{90}Y-microsphere SIRT in HCC patients at our center has been reported [33]. Although ^{90}Y PET/CT has gained increasing interest for post-treatment evaluation of ^{90}Y microsphere distribution [34, 35], offering better spatial resolution imaging and more accurate dosimetry parameters compared to SPECT/CT, this particular imaging modality was not included in the scope of our study.

There were several factors affecting the dosimetry of ^{90}Y SIRT, driven by patient-specific characteristics and various procedural aspects. These factors include the differences in imaging workflows between MAA and resin microspheres, potential catheter position deviations, variations in tumoral-liver characteristics and volumes among patients, the influence of LSF and TLR, as well as differences between the imaging modalities utilized. One main limitation of this study was related to the segmentation of VOIs for dosimetry methods, particularly in delineating tumoral-liver regions. This task was challenging due to discrepancies between pre-SIRT and post-SIRT dose estimates and the nature of indistinct boundary of tumors in nuclear medicine imaging [36]. Nevertheless, the study addressed this limitation by employing semi-automated delineation from MIM Encore software, a radionuclide therapy treatment planning software, and subsequently validating the contouring by both nuclear medicine physician and interventional radiologist. This approach aimed to improve the accuracy of tumoral-liver region delineation, especially for cases with equivocal tumor margins, and enhance the precision of dosimetry calculations for clinical use. However, this study did not evaluate the interobserver variability in segmentation between a certified nuclear medicine physician and an interventional radiologist for both tumoral-liver and non-tumoral liver VOI, since the definition of these regions relied on a consensus agreement between the two according to our routine protocol, resulting in no observed disagreement. We acknowledge this limitation in our study. To further enhance dosimetry accuracy for SIRT liver radioembolization, it is recommended to include a whole-lung SPECT/CT scan. This additional imaging step can improve the accuracy of LSF calculation, which is critical for optimizing treatment planning and maximizing therapeutic outcomes.

Conclusions

Despite the differences in absorbed doses, ^{99m}Tc-MAA SPECT/CT remains a suitable pre-treatment planning tool for predicting the distribution of ^{90}Y-microspheres in both tumoral-liver and non-tumoral liver regions. It is important to note that while the quantitative analysis obtained from ^{90}Y-bremsstrahlung SPECT/CT images has its limitations in terms of image quality, it still provides valuable visualization of the intrahepatic and extrahepatic distribution of injected ^{90}Y-microspheres radioembolization for hepatocellular carcinoma patients. The correlation between ^{99m}Tc-MAA and ^{90}Y-bremsstrahlung SPECT/CT can be highly beneficial for interventional radiologists in providing personalized dosimetry planning in ^{90}Y radioembolization treatment using the partition model.

Declarations

Conflict of interest The authors declare that they have no conflicts of interest.

References

1. Sung H, Ferlay J, Siegel RL, Laversanne M, Soerjomataram I, Jemal A, et al. Global cancer statistics 2020: GLOBOCAN estimates of incidence and mortality worldwide for 36 cancers in 185 countries. CA Cancer J Clin. 2021;71(3):209–49.
2. Arnold M, Abnet CC, Neale RE, Vignat J, Giovannucci EL, McGlynn KA, et al. Global burden of 5 major types of gastrointestinal cancer. Gastroenterology. 2020;159(1):335–49. e15.
3. Saeku S, Noipinit N, Khamwan K, Siricharoen P. Liver and tumor segmentation in selective internal radiation therapy ^{99m}Tc-MAA SPECT/CT images using MANet and histogram adjustment. In: 3rd Asia Symposium on Signal Processing (ASSP). IEEE, 2022, pp 62–66.
4. Kim SP, Cohalan C, Kopek N, Enger SA. A guide to ^{90}Y radioembolization and its dosimetry. Phys Med. 2019;68:132–45.
5. Weber M, Lam M, Chiesa C, Konijnenberg M, Cremonesi M, Flamen P, et al. EANM procedure guideline for the treatment of liver cancer and liver metastases with intra-arterial radioactive compounds. Eur J Nucl Med Mol Imaging. 2022;49(5):1682–99.
6. Riveira-Martin M, Akhavanallaf A, Mansouri Z, Bianchetto Wolf N, Salimi Y, Ricoeur A, et al. Predictive value of ^{99m}Tc-MAA-based dosimetry in personalized ^{90}Y-SIRT planning for liver malignancies. EJNMMI Res. 2023;13(1):63.

7. Chiesa C, Sjogreen-Gleisner K, Walrand S, Strigari L, Flux G, Gear J, et al. EANM dosimetry committee series on standard operational procedures: a unified methodology for ^{99m}Tc-MAA pre-and ^{90}Y peri-therapy dosimetry in liver radioembolization with ^{90}Y microspheres. EJNMMI Phys. 2021;8(1):77.

8. Bayat Z, Saeedzadeh E, Vahidfar N, Sadeghi M, Farzenefar S, Daha FJ, et al. Preparation and validation of [^{67}Ga] Ga-phytate kit and Monte Carlo dosimetry: an effort toward developing an impressive lymphoscintigraphy tracer. J Radioanal Nucl Chem. 2022;331(2):691–700.

9. Heidari S, Sadeghi M, Akhlaghi M, Beiki D, Yazdi SI. Internal dosimetry of ^{64}Cu-DOX-loaded microcapsules by Monte Carlo method. Appl Radiat Isot. 2023;196: 110788.

10. Yazdi SI, Sadeghi M, Saeedzadeh E, Jalilifar M. Radiation dosimetry of ^{89}Zr labeled antibody estimated using the MIRD method and MCNP code. Nucl Eng Technol. 2023;55(4):1265–8.

11. Khamwan K, Krisanachinda A, Pasawang P. The determination of patient dose from ^{18}F-FDG PET/CT examination. Radiat Prot Dosim. 2010;141(1):50–5.

12. Prompers L, Bucerius J, Brans B, Temur Y, Berger L, Mottaghy FM. Selective internal radiation therapy (SIRT) in primary or secondary liver cancer. Methods. 2011;55(3):253–7.

13. Sahafi-Pour SA, Shirmardi SP, Saeedzadeh E, Baradaran S, Sadeghi M. Internal dosimetry studies of ^{177}Lu-BBN-GABA-DOTA, as a cancer therapy agent, in human tissues based on animal data. Appl Radiat Isot. 2022;186: 110273.

14. Dalvand S, Sadeghi M. Bone marrow dosimetry for ^{141}Ce-EDTMP as a potential bone pain palliation complex: a Monte Carlo study. Appl Radiat Isot. 2022;182: 110113.

15. Chatachot K, Shiratori S, Chaiwatanarat T, Khamwan K. Patient dosimetry of ^{177}Lu-PSMA I&T in metastatic prostate cancer treatment: the experience in Thailand. Ann Nucl Med. 2021;35:1193–202.

16. Villalobos A, Cheng B, Wagstaff W, Sethi I, Bercu Z, Schuster DM, et al. Tumor-to-normal ratio relationship between planning Technetium-99 macroaggregated albumin and posttherapy Yttrium-90 Bremsstrahlung SPECT/CT. J Vasc Interv Radiol. 2021;32(5):752–60.

17. Nezami N, Kokabi N, Camacho JC, Schuster DM, Xing M, Kim HS. ^{90}Y radioembolization dosimetry using a simple semi-quantitative method in intrahepatic cholangiocarcinoma: glass versus resin microspheres. Nucl Med Biol. 2018;59:22–8.

18. Gallio E, Richetta E, Finessi M, Stasi M, Pellerito RE, Bisi G, et al. Calculation of tumour and normal tissue biological effective dose in ^{90}Y liver radioembolization with different dosimetric methods. Phys Med. 2016;32(12):1738–44.

19. Ho S, Lau W, Leung T, Chan M, Ngar Y, Johnson P, et al. Partition model for estimating radiation doses from yttrium-90 microspheres in treating hepatic tumours. Eur J Nucl Med. 1996;23(8):947–52.

20. Cremonesi M, Chiesa C, Strigari L, Ferrari M, Botta F, Guerriero F, et al. Radioembolization of hepatic lesions from a radiobiology and dosimetric perspective. Front Oncol. 2014;4:210.

21. Kao YH, Tan AEH, Burgmans MC, Irani FG, Khoo LS, Lo RHG, et al. Image-guided personalized predictive dosimetry by artery-specific SPECT/CT partition modeling for safe and effective ^{90}Y radioembolization. J Nucl Med. 2012;53(4):559–66.

22. Levillain H, Bagni O, Deroose CM, Dieudonné A, Gnesin S, Grosser OS, et al. International recommendations for personalised selective internal radiation therapy of primary and metastatic liver diseases with yttrium-90 resin microspheres. Eur J Nucl Med Mol Imaging. 2021;48(5):1570–84.

23. Roosen J, Klaassen NJ, Westlund Gotby LE, Overduin CG, Verheij M, Konijnenberg MW, et al. To 1000 Gy and back again: a systematic review on dose-response evaluation in selective internal radiation therapy for primary and secondary liver cancer. Eur J Nucl Med Mol Imaging. 2021;48(12):3776–90.

24. Chansanti O, Jahangiri Y, Matsui Y, Adachi A, Geeratikun Y, Kaufman JA, et al. Tumor dose response in yttrium-90 resin microsphere embolization for neuroendocrine liver metastases: a tumor-specific analysis with dose estimation using SPECT-CT. J Vasc Interv Radiol. 2017;28(11):1528–35.

25. Gnesin S, Canetti L, Adib S, Cherbuin N, Monteiro MS, Bize P, et al. Partition model–based ^{99m}Tc-MAA SPECT/CT predictive dosimetry compared with ^{90}Y TOF PET/CT posttreatment dosimetry in radioembolization of hepatocellular carcinoma: a quantitative agreement comparison. J Nucl Med. 2016;57(11):1672–8.

26. Chiesa C, Mira M, Maccauro M, Spreafico C, Romito R, Morosi C, et al. Radioembolization of hepatocarcinoma with ^{90}Y glass microspheres: development of an individualized treatment planning strategy based on dosimetry and radiobiology. Eur J Nucl Med Mol Imaging. 2015;42(11):1718–38.

27. Haste P, Tann M, Persohn S, LaRoche T, Aaron V, Mauxion T, et al. Correlation of technetium-99m macroaggregated albumin and yttrium-90 glass microsphere biodistribution in hepatocellular carcinoma: a retrospective review of pretreatment single photon emission CT and posttreatment positron emission tomography/CT. J Vasc Interv Radiol. 2017;28(5):722–30. e1.

28. Ilhan H, Goritschan A, Paprottka P, Jakobs TF, Fendler WP, Todica A, et al. Predictive value of ^{99m}Tc-MAA SPECT for ^{90}Y-labeled resin microsphere distribution in radioembolization of primary and secondary hepatic tumors. J Nucl Med. 2015;56(11):1654–60.

29. Ahmadzadehfar H, Muckle M, Sabet A, Wilhelm K, Kuhl C, Biermann K, et al. The significance of bremsstrahlung SPECT/CT after yttrium-90 radioembolization treatment in the prediction of extrahepatic side effects. Eur J Nucl Med Mol Imaging. 2012;39(2):309–15.

30. Brosch J, Gosewisch A, Kaiser L, Seidensticker M, Ricke J, Zellmer J, et al. 3D image-based dosimetry for Yttrium-90 radioembolization of hepatocellular carcinoma: impact of imaging method on absorbed dose estimates. Phys Med. 2020;80:317–26.

31. Elschot M, Vermolen BJ, Lam MG, de Keizer B, van den Bosch MA, de Jong HW. Quantitative comparison of PET and Bremsstrahlung SPECT for imaging the in vivo yttrium-90 microsphere distribution after liver radioembolization. PLoS ONE. 2013;8(2): e55742.

32. Levillain H, Duran Derijckere I, Ameye L, Guiot T, Braat A, Meyer C, et al. Personalised radioembolization improves outcomes in refractory intra-hepatic cholangiocarcinoma: a multicenter study. Eur J Nucl Med Mol Imaging. 2019;46(11):2270–9.

33. Chaikajornwat J, Tanasoontrarat W, Phathong C, Pinjaroen N, Chaiteerakij R. Clinical outcome of Yttrium-90 selective internal radiation therapy (Y-90 SIRT) in unresectable hepatocellular carcinoma: experience from a tertiary care center. Liver Res. 2022;6(1):30–8.

34. Richetta E, Pasquino M, Poli M, Cutaia C, Valero C, Tabone M, et al. PET-CT post therapy dosimetry in radioembolization with resin ^{90}Y microspheres: comparison with pre-treatment SPECT-CT ^{99m}Tc-MAA results. Phys Med. 2019;64:16–23.

35. Song YS, Paeng JC, Kim H-C, Chung JW, Cheon GJ, Chung J-K, et al. PET/CT-based dosimetry in ^{90}Y-microsphere selective internal radiation therapy: single cohort comparison with pretreatment planning on ^{99m}Tc-MAA imaging and correlation with treatment efficacy. Medicine. 2015;94(23): e945.

36. Khamwan K, Krisanachinda A, Pluempitiwiriyawej C. Automated tumour boundary delineation on ^{18}F-FDG PET images using active contour coupled with shifted-optimal thresholding method. Phys Med Biol. 2012;57(19):5995–6005.